



Support of Dynamic Measurements Through Similitude Formulations

A. Casaburo¹ · G. Petrone¹ · V. Meruane² · F. Franco¹ · S. De Rosa¹

Received: 23 October 2020 / Accepted: 27 February 2021
© The Author(s) 2021

Abstract

Up to now, similitude methods have been used in order to overcome the typical drawbacks of experimental testing and numerical simulations by reconstructing the full-scale model behavior from that of the scaled model. The novelty of this work is the application of similitude theory not as a tool for predicting the prototype dynamic response, but for supporting, and eventually validating, experimental measurements polluted by noise. Two Aluminium Foam Sandwich (AFS) plates are analyzed with Digital Image Correlation (DIC) cameras. First, an algorithm for blind source separation problems is used to extract information about the excitation; then, SAMSARA (Similitude and Asymptotic Models for Structural-Acoustic Research Applications) similitude method is applied to both the force spectra and velocity responses of prototype and model. The reconstruction of force and velocity curves demonstrates that the similitude results are coherent with the quality of the experimental measurements: when the spatial pattern in resonance is recognizable, then the curves overlap. Instead, when the displacement field of just one model is not well identified, the reconstruction exhibits discrepancies. Therefore, similitude methods reveal to be an interesting tool for understanding if a set of measurements is reliable or not and their application should not be underestimated, especially in the light of the expanding range of approaches which can extract important information from noisy observations.

Keywords Similitude · Sandwich plates · Modal analysis · Digital image correlation

Introduction

The increasing complexity of modern engineering systems makes uneasy to carry out all types of analyses, may they

be analytical, numerical or experimental, especially in structural dynamics. In fact, on the one hand, laboratory experiments may be expensive, time consuming, as well as hard to setup when the test article has too large (or too small) dimensions. On the other hand, analytical and numerical simulations may be computationally prohibitive.

In recent years, similitude theory has provided interesting tools, the similitude methods, which allow to derive the conditions to design a scaled-up or down model of the full-scale prototype, and the scaling laws to reconstruct the behavior of the prototype from that of the model (or vice versa) at best. Therefore, applying these sets of conditions and scaling laws, one can assemble a specimen much easier to test, as well as move towards analytical or numerical domains which resolution is computationally more efficient.

There are many reviews on similitude theory [8, 12, 35, 39] that may be useful to the interested reader. These works highlight that there are some well-established methods that have been used up to now. The most important is DA (Dimensional Analysis), based on Buckingham's Π Theorem, introduced in engineering field by Goodier and Thomson [20]. The method allows to derive dimensionless

✉ A. Casaburo
alessandro.casaburo@unina.it

G. Petrone
giuseppe.petrone@unina.it

V. Meruane
vmeruane@uchile.cl

F. Franco
francof@unina.it

S. De Rosa
sergio.derosa@unina.it

¹ Pasta-Lab, Department of Industrial Engineering, Università degli Studi di Napoli "Federico II", Via Claudio 21, Naples, 800125, Italy

² Department of Mechanical Engineering, Universidad de Chile, Beauchef 850, Santiago De Chile, Chile



groups made of the parameters governing the phenomenon under investigation. Then, STAGE (Similitude Theory Applied to Governing Equations), introduced by Kline [24], which derives similitude conditions and scaling laws by directly inserting the scale factors into the governing equations. It is widely applied by Simites and Rezaeepazhand to composite plates [34] and cylinders [30], expanding the type of structural configurations and loading conditions in successive works. The versatility of STAGE is demonstrated with applications to other structural configurations and engineering problems, for example to investigate the dynamic response [3, 4] and the strain field [2] of laminated beams, as well as the dynamic behavior stiffened cylinders [36].

A change of paradigm is introduced with the energy methods. The first, up to Kasivitamnuay and Singhatandig [23], is based on the principle of energy conservation. Successively, De Rosa et al. [16] address the computational problems, associated to FEA (Finite Element Analysis), with ASMA (Asymptotical Modal Scaled Analysis), which aims at reducing the extension of the geometrical parameters not involved into energy transmission in order to retain the original finite element mesh and increase the computational efficiency of FEM (Finite Element Method). Then, De Rosa et al. [15] lay the bases for SAMSARA, a generalization of the modal approach used in ASMA, which allows to enlarge the number of parameters to investigate the similitude of acoustic-structural systems. Recently, Casaburo et al. [9] have investigated the potentialities of machine learning methods in similitude field by applying artificial neural networks to SAMSARA framework.

Finally, last years have seen the introduction of SA (Sensitivity Analysis) into similitude field. The first to introduce it are Luo et al. [26], which couple the application of STAGE with a set of principles, based on sensitivity analysis. Then, Adams et al. [1] apply SA to derive sensitivity-based scaling laws, as opposed to similitude-based scaling laws. By doing so, the authors can derive the scaling laws without a previous knowledge of the scaling behavior of the system under analysis.

The main objective of these works is to obtain a very good prediction of the prototype behavior by re-scaling the response of a model, properly designed. Some of them, like Simites and Rezaeepazhand [34], investigate different combinations of scale factors to find the distorted model which returns the best prototype prediction, or to get distorted scaling laws giving satisfactory predictions with a value of discrepancy fixed *a priori* [26]. These analyses become mandatory because not always the experimental facilities can house the models, as well as some similitude conditions may require the development of geometrical dimensions beyond the capabilities of today's technology. Also manufacturing errors play an important role in this

regard. However, even in these cases, both the approach and the results are addressed towards the final comparison with the prototype results.

When the similitude conditions are satisfied, it is expected that the prototype curve and the model scaled curve almost overlap. The reconstruction of the prototype curve from that of the model through the scale factors and scaling laws is called *remodulation*. Therefore, as already noted in the work by Franco et al. [19], dedicated to the investigation of plates in similitude excited by TBL (Turbulent Boundary Layer), similitude theory may provide information about the quality of the experimental test, typically affected by uncertainties, random noise and errors due to other sources, by observing the quality of the remodulation process.

Following this idea, similitude methods can be applied for other purposes than the typical ones reported in literature (namely, predict the behavior of the full-scale model). The fact that the curves of two models are bound to overlap, when certain conditions are fulfilled, can be used to support experimental measurements polluted by uncertainties, provide a criterion to decide whether a laboratory experiment is acceptable or not, and understand to which extent noisy or missing data affects the remodulation.

For example, a campaign of experimental tests on a particular structure may turn out to be polluted by noise. Before proceeding to another experimental campaign (with its own financial and temporal costs) or, more generally, taking decisions or drawing conclusions on the behavior of the structure on the basis of these results, it would be useful to perform a remodulation, by means of scaling laws, and compare them with a set of reference measurements, considered reliable, executed on a structure of the same type but different dimensions. The level of discrepancy between the reference curves and the remodulated ones may help to take a final decision concerning the non-acceptance of the results. The approach may be even more useful when alternative validation procedures, like analytical solutions or numerical simulations, are missing or take too much time, since the remodulation process can be executed in few seconds.

Therefore, SAMSARA method is herein applied to corroborate the measurements obtained by means of a DIC test on two metallic foam sandwich panels, in complete similitude, excited by a shaker. The main objective of this investigation is, by comparing the experimental measurements of systems in similitude with different levels of noise, to demonstrate that it is possible to establish whether a set of measurements is reliable or not. The reconstruction of the response, as well as the validation of measurements in presence of noise, have been widely investigated in literature. Two works worth of mention are the one by Chen et al. [11], who propose a method for expanding the dynamic response

from a sparse set of points to a much larger set without utilizing a finite element model, and the article by Chen et al. [10], in which the authors propose a function to check the consistencies of measurements to all of the data of the entire set.

The investigation of structural stress and vibrations is widely executed with DIC cameras. In fact, they allow to collect quite quickly high-density spatial information from structures remotely. This is an advantage in all those cases in which contact sensors may induce mass-loading effects (like lightweight structures), or the large scale of the test article implies long sessions of intensive human work and result time consuming. Sarrafi et al. [31] apply Phase-based Motion Estimation (PME) and video magnification to execute an operational modal analysis on turbine blades aiming at executing vibration-based SHM (Structural Health Monitoring). Recently, [38] have combined DIC and Element-free Galerkin (EFG) to characterize the strain field and extracting the stress intensity factor of a surface crack.

DIC measurements are bounded by intrinsic limitations, that are the sources of errors and uncertainties, such as the precision of the cameras and the errors. Camera precision is linked to the pixel dimension: the displacement of a point can be registered only if it crosses the borders of the pixel. Regarding the errors, there are two types [32, 33]: correlation and calibration errors. The latter impacts the reconstruction of the 3D coordinates of the points. The former can be divided into two contributions: statistical and systematic errors. The analysis and reduction of errors are the main topic of many works. For example, Jones et al. [22] propose X-ray imaging in place of optical imaging when the refraction of visible light, due to density gradients between DIC cameras and the test article (generated by smoke, flame, heated object, shock waves due to explosions, etc.) generates a substantial error that can invalidate the measurement itself. The work by Li et al. [25] concerns the discrepancy between the order of the real deformation and that of the applied mapping function in experimental tests involving DIC cameras.

However, in general not all the error sources present in image correlation techniques are under the control of the analyzer: not all the results directly provided by the cameras can be used, therefore they needed some post-processing to reconstruct the vibrational responses. These responses are directly extracted from the experimental measurements provided by the DIC camera or with the aid of a SOBI (Second-Order Blind Identification) algorithm [21].

This work is set in a wider framework aiming at the analysis of metallic foam sandwich configurations in similitude. The sandwich plates tested in this work are manufactured and sold by the Austrian company Mepura Metallpulver GmbH and have commercial name Alulight®. The material properties are defined by D'Alessandro et al.

[14], while the vibroacoustic properties are investigated by Petrone et al. [28]. Up to now, these plates have never been analysed in the context of similitude theory.

The article is organized as follows. Section “**Theoretical Framework**” summarizes the theoretical framework. First, the SAMSARA method is applied to derive the similitude conditions and natural frequencies of both simply supported isotropic and AFS plates. Then, the scaling law of the velocity response and the mobility are derived. Finally, the steps of the SOBI algorithm are listed. In Section “**Results**”, SOBI algorithm and SAMSARA are applied to numerical plates to understand to which extent the noise affects the performances of the methods. Then, SOBI algorithm is used on experimental data to reconstruct the spectra of the excitation forces and to estimate the scale factor of force amplitude. Finally, SAMSARA is used as validation method of DIC measurements by overlapping the prototype and proportional sides curves. Final remarks are summarized in the last Section, “**Conclusions and Further Research**”.

Theoretical Framework

In this section, the similitude method is first explained. Then, the tools necessary for the analytical reconstruction of the FRF (Frequency Response Function) are briefly explained. Finally, the scheme of the SOBI algorithm is listed.

Similitude Method

The similitude method herein used is SAMSARA, which details can be found in De Rosa et al. [17]. For any parameter of the system (prototype), g , it is possible to define a scale factor

$$r_g = \frac{\hat{g}}{g}, \quad (1)$$

where the hat symbol characterizes the model parameters. In the successive sections, the similitude conditions and scaling laws of natural frequencies and velocity response are derived for both isotropic and aluminium foam sandwich plates with simply supported boundary conditions.

Isotropic plate

The equation of natural frequencies of the prototype isotropic simply supported plate is [7]

$$\omega_{mn} = \pi^2 \sqrt{\frac{Eh^2}{12\rho(1-\nu^2)}} \left[\left(\frac{m}{a}\right)^2 + \left(\frac{n}{b}\right)^2 \right]. \quad (2)$$

The parameters a and b are the length and the width of the panel, respectively, h the thickness, E the Young's modulus,

ρ the mass density per unit volume, and ν the Poisson's ratio. Finally, m and n are the number of half waves in x and y directions, characterizing the mode order and, thus, the spatial pattern at the considered frequency.

The behavior of scaled-up or down models are described by the same equations characterizing the prototype; therefore equation (2) holds for models, too. By expliciting the model parameters in terms of scale factor and prototype parameter, according to equation (1), the natural frequencies of the model can be written as

$$r_\omega \omega_{mn} = \pi^2 \sqrt{\frac{r_E E r_h^2 h^2}{12 r_\rho \rho (1 - \nu^2)}} \left[\left(\frac{m}{r_a a} \right)^2 + \left(\frac{n}{r_b b} \right)^2 \right], \quad (3)$$

in which it is assumed that the Poisson's ratio does not change ($r_\nu = 1$) and that, when considering natural frequencies of the same order, neither the number of half waves change.

Equations (2) and (3) are the same if

$$r_\omega = \sqrt{\frac{r_E}{r_\rho} \frac{r_h}{r_a^2}} = \sqrt{\frac{r_E}{r_\rho} \frac{r_h}{r_b^2}}. \quad (4)$$

The equalities reported in equation (4) are true at the same time if, and only if,

$$r_a = r_b. \quad (5)$$

Equation (5) is the similitude condition for the complete similitude of isotropic plates, according to which the length and the width must scale in the same way. Equivalently, the aspect ratio of the panel must not change. Fulfilling equation (5) leads to a true model - or *proportional sides* model - which allows an accurate reconstruction of the prototype response by applying the univocal scaling law

$$r_\omega = \sqrt{\frac{r_E}{r_\rho} \frac{r_h}{r_L^2}}, \quad (6)$$

where $r_L = r_a = r_b$. Equation (6) descends directly from equation (4) when equation (5) is fulfilled, and provides the scale factor to use for predicting the natural frequencies of the prototype from those of the model. Moreover, equation (6) shows that material properties and thickness are free (or unconstrained) parameters, because their values are not constrained by any similitude condition.

Sandwich plate

The equation of the natural frequencies of the full-scale simply supported sandwich plate is provided by Vinson [37]

$$\omega_{mn} = \frac{\pi^2}{a^2} \sqrt{\frac{D}{\rho_S}} \sqrt{m^4 + 2m^2 n^2 \left(\frac{a}{b} \right)^2 + n^4 \left(\frac{a}{b} \right)^4}, \quad (7)$$

where D is the bending stiffness and ρ_S is the mass density per unit area. The other symbols have the same meaning previously described.

The bending stiffness needs characterization for a sandwich configuration. According to Powell and Stephens, [29], if the sandwich plate has both facings and core made of isotropic material, then the bending stiffness can be divided into two contributes: one associated with the face sheets, the other to the core:

$$D = \frac{E_f (h^3 - h_c^3)}{12(1 - \nu_f^2)} + \frac{E_c h_c^3}{12(1 - \nu_c^2)}, \quad (8)$$

where the subscripts f and c refer to facing and core, respectively.

Applying the procedure of the previous subsection, expliciting the mass density per unit area but not the bending stiffness, then the equation of natural frequencies of any model is given by

$$r_\omega \omega_{mn} = \frac{\pi^2}{r_a^2 a^2} \sqrt{\frac{r_D D r_a a r_b b}{r_M M}} \sqrt{m^4 + 2m^2 n^2 \left(\frac{r_a a}{r_b b} \right)^2 + n^4 \left(\frac{r_a a}{r_b b} \right)^4}, \quad (9)$$

with M being the total mass of the plate.

Once more, equations (7) and (9) are the same if

$$r_\omega = \frac{1}{r_a^2} \sqrt{\frac{r_D r_a r_b}{r_M}} = \frac{1}{r_a r_b} \sqrt{\frac{r_D r_a r_b}{r_M}} = \frac{1}{r_b^2} \sqrt{\frac{r_D r_a r_b}{r_M}}, \quad (10)$$

from which it is straightforward to deduce that the similitude condition for sandwich plates in complete similitude is the same of isotropic plates, reported in equation (5): $r_a = r_b$. The univocal scaling law of natural frequencies shall take the form

$$r_\omega = \frac{1}{r_L} \sqrt{\frac{r_D}{r_M}}, \quad (11)$$

in which possible changes in material properties are automatically taken into account by the bending stiffness scale factor, r_D .

Velocity response

According to the modal approach, the velocity response of a linear system is the sum of its vibration modes [13]; therefore, the prototype velocity is given by

$$V(x_F, x_R; \omega) = j\omega F(\omega) \sum_{m=1}^{\infty} \sum_{n=1}^{\infty} \frac{\phi_{mn}(x_F) \phi_{mn}(x_R)}{\mu_{mn} [\omega_{mn}^2 - \omega^2 + j\eta \omega_{mn}^2]}. \quad (12)$$

In equation (12), x_F and x_R are the dimensionless excitation and measurement points, respectively, j the imaginary unit, ϕ_{mn} is the mode shape of order (m, n) , $F(\omega)$ is the harmonic force acting in x_F , and η the damping loss factor.

The term μ_{mn} is the generalized mass that, for any simply supported plate, can be written as

$$\mu_{mn} = \rho h \int_0^a \int_0^b \phi_{mn}^2(x, y) dx dy = \frac{M}{4}. \quad (13)$$

Therefore, all the mode shapes are associated to the same generalized mass.

Considering that the generalized mass scale factor can be written in terms of mass scale factor (because of equation (13)), and assuming unchanged damping ($r_\eta = 1$), the model velocity response can be written as

$$r_V V(x_F, x_R; r_\omega \omega) = \frac{j r_\omega \omega r_F F(r_\omega \omega)}{r_M \mu_{mn}} \sum_{m=1}^{\infty} \sum_{n=1}^{\infty} \frac{\phi_{mn}(x_F) \phi_{mn}(x_R)}{r_\omega^2 (\omega_{mn}^2 - \omega^2 + j \eta \omega_{mn}^2)}, \quad (14)$$

from which, the velocity scales according to the law

$$V(x_R, x_F; \omega) = \frac{r_M r_\omega}{r_F} \widehat{V}(x_R, x_F; r_\omega \omega). \quad (15)$$

Thus, it is possible to conclude that equation (12) does not generate any similitude condition, only the scaling law given by equation (15).

First of all, in equation (14) the mode shapes do not need scaling, being dimensionless and normalized representations of the same vibration patterns. For the same reason, neither the dimensionless excitation and measurement points, x_F and x_R , scale. Equation (15), instead, shows that the prediction of the velocity from one model to another is carried out in two steps. Firstly, the velocity amplitude is scaled by the term $\frac{r_M r_\omega}{r_F}$. Then, the resonance peaks are aligned in frequency by means of the term $r_\omega \omega$. Thus, there is, first, a remodulation in amplitude, then in frequency.

If, instead of velocity, mobility is considered,

$$Y = \frac{V(x_F, x_R; \omega)}{F(\omega)} = j \omega \sum_{m=1}^{\infty} \sum_{n=1}^{\infty} \frac{\phi_{mn}(x_F) \phi_{mn}(x_R)}{\mu_{mn} [\omega_{mn}^2 - \omega^2 + j \eta \omega_{mn}^2]}, \quad (16)$$

it is straightforward to demonstrate that the mobility scales as

$$r_Y = \frac{1}{r_M r_\omega}. \quad (17)$$

Equation (17) directly descends from equations (15) and (16), therefore the same considerations hold.

The actual analysis has considered simply-supported boundary conditions. According to the proposed modal approach, the above relationships are still valid if the prototype and the model have the same boundary conditions, independently from their specific characteristics (clamped, pinned, etc.).

SOBI Algorithm

In some experimental set-ups, even though force transducers are used, the spectra of the excitation load can be unknown. This may happen for several reasons, such as uncertainties on the measurements, impossibility to measure the exciting load, etc. Under these circumstances, an alternative way would be to identify the dynamic loads indirectly by the measured structural dynamic responses.

In the present work, the spectra of the exciting forces are determined by means of a SOBI algorithm. This class of algorithms are typically used to solve BSS (Blind Source Separation) problems, in which a series of independent source signals are recovered from a set of mixed signals, without any prior knowledge about the source signals. The SOBI algorithm herein used is proposed by Jia et al. [21], which is an extension to the prediction of random dynamic loads of the algorithm due to McNeill and Zimmerman [27]. Providing the analytical details of the algorithm is outside the aims of this work, however the computational steps are further listed to give an idea of the involved parameters:

1. Obtain the structural response (time history of points displacements).
2. Evaluation of the PSD (Power Spectral Density) matrix of the structural response.
3. Estimation of the modal matrix, modal damping ratio, and natural frequencies.
4. Calculation of the PSD matrix of modal responses.
5. Evaluation of the $\mathbf{Z}_\phi(\omega)$ and modal loads PSD matrices.
6. Estimation of the random dynamic load PSD matrix.

The matrix $\mathbf{Z}_\phi(\omega)$ is a diagonal matrix which i -th element is

$$Z_i = \mu_i (\omega_i^2 - \omega^2 + j \eta_i \omega_i^2), i = 1, 2, \dots, N \quad (18)$$

being N the total number of degrees of freedom. Equation (18) can be easily recognized as the denominator of the transfer function.

Results

In this section, the results provided by similitude theory are reported. The core of this work is summarized in the flowchart of Fig. 1, in which the rectangular red frames are assigned to experimental procedures and results, while those rounded blue are associated to numerical/analytical procedures and results.

The experimental displacement time histories, provided by the DIC measurements, along with the natural frequencies experimentally determined by means of previous accelerometric tests, are given as input to the SOBI algorithm described in “[Similitude Method](#)”, which extracts the

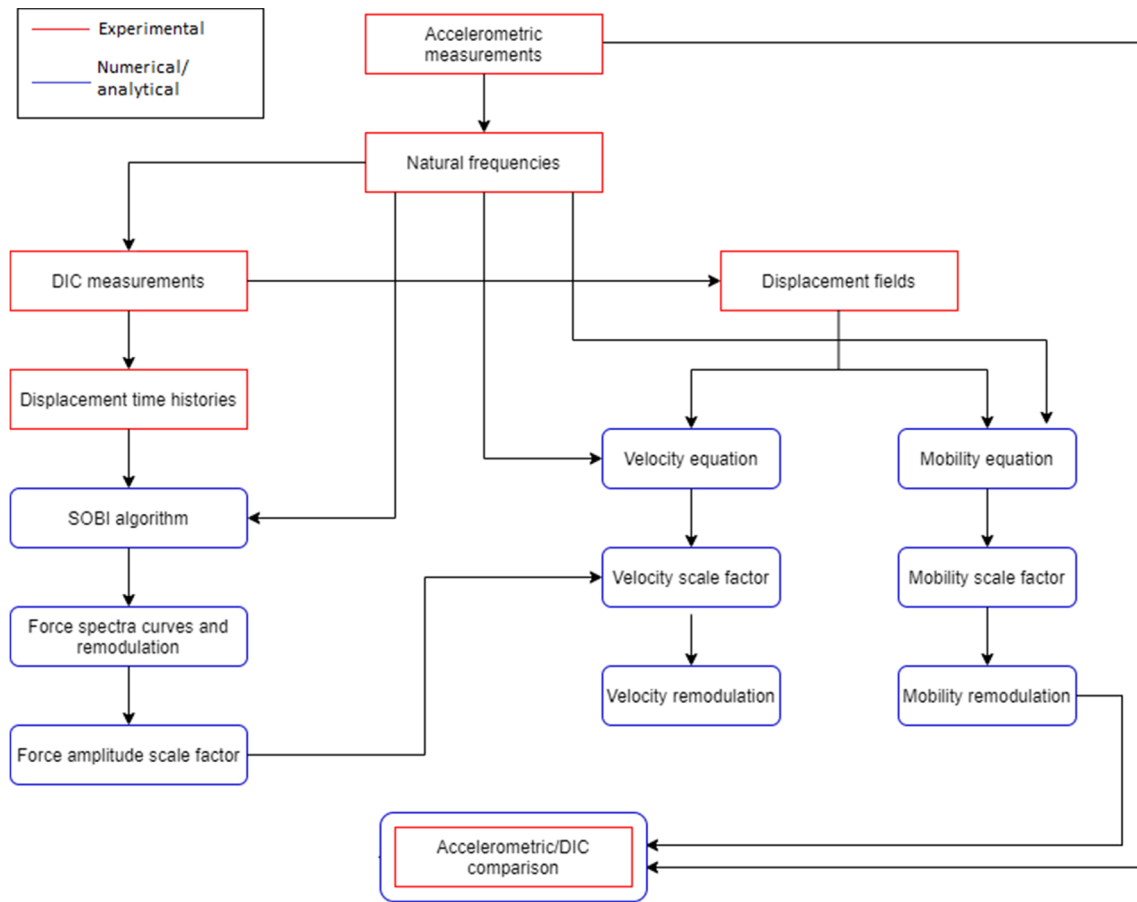


Fig. 1 Work flowchart

spectra of the excitation forces. In this way, it is possible to understand whether the input information is coherently retained into noisy data and derive the force amplitude scale factor, used further to calculate the velocity scale factor. This scale factor allows the remodulation in both frequency and amplitude of the velocity curves, analytically evaluated starting from the displacement fields provided by DIC cameras and the experimental natural frequencies, according to equation (12). Therefore, it is possible to determine if the experimental estimation of the displacements for each mode is acceptable or not. Finally, the same operation is executed with the mobility (equation (16)), then compared with the accelerometric observations, in order to understand if all the analytical calculations carried out are, generally, correct and coherent.

In the next sections, the proposed approach is initially applied to results numerically derived for sake of completeness and clarity. In particular, data is polluted with random Gaussian noise to investigate the effect of uncertainties on the results. Successively, the procedure is applied to a real, more complex, laboratory case.

Numerical Plates

Two simply supported isotropic aluminium plates are numerically investigated: a prototype (P) and a proportional sides model (PS). Their geometrical details and the mass of each plate are listed in Table 1, while the material properties, which do not change between the models, are summarized in Table 2. Table 3 reports the scale factor necessary for the analysis, obtained from the geometrical and material properties of the models, as well as from the application of equations (6) and (15). It is assumed that both the Poisson's ratio and the damping do not change, which is

Table 1 Geometrical characteristics and mass of the prototype and the proportional sides model

	a [m]	b [m]	t[m]	M [kg]
P	0.656	0.476	0.003	2.53
PS	0.558	0.405	0.003	1.83

Table 2 Material properties

Young's modulus, E	71 GPa
Mass density, ρ	2700 kg/m ³
Poisson's ratio, ν	0.33
Structural loss factor, η	0.001

an acceptable hypothesis if the material properties and the boundary conditions are the same between the models.

The numerical models are made with PSHELL property and QUAD elements. The numerical mesh presents 88 points (11 along the x direction, 8 along the y direction), as shown in Fig. 2.

Both the plates are excited with several sinusoidal forces, applied once at time, with frequencies equal to the natural frequencies of the test articles. The prototype and the model are subjected to forces with amplitudes equal to 2 N and 1 N, respectively. Therefore, the scale factors of the force amplitude and the PSD are $r_F = 0.5$ and $r_{SFF} = 0.25$.

The SOBI algorithm introduced in “[Similitude Method](#)” is herein used to derive the force PSD from the plates displacements. If the PSD curves remodulate according to the scale factor, then the similitude holds and the algorithm is reliable. It is reasonable to assume that the procedure can be applied even for cases in which not all the information about the excitation is known.

In this regard, the force PSD associated to the first two modes are evaluated. For each mode, the time history of the displacement of each point is polluted with random Gaussian noise having 1%, 5%, and 10% of standard deviation σ , in order to investigate the behavior of the algorithm in presence of increasing levels of uncertainties.

With reference to the list in “[Similitude Method](#)”, the structural responses needed in step 1 are numerically derived, then polluted with noise. The evaluation of the modal matrix in step 3 is carried out with the JAD (Joint Approximated Diagonalization) method of the whitened response covariance matrix. The algorithm to perform this operation is provided by Belouchrani et al. [6].

Fig. 3 shows the force PSD remodulation when the excitation frequency is equal to the first natural frequency. In each figure, three curves are plotted. The blue curve

represents the force PSD of the prototype, the red curve the force PSD of the proportional sides, and the yellow curve the force PSD of the proportional sides remodulated in frequency and amplitude. Each figure displays a small box which focuses on the peaks. All the figures demonstrate that the amplitude remodulations carried out with the scale factors predicted are accurate. However, passing from 1% (Fig. 3(a)) to 10% (Fig. 3(c)) of standard deviation, there is a sensitive decrease of PSD amplitude. Therefore, the loss of information due to noise exhibits in terms of underestimated amplitude. Nonetheless, the scaling procedure is still valid.

The results of Fig. 3 make clear that the SOBI algorithm allows to derive coherent excitation information even though the measurements are noisy. The input frequency is set on the basis of the natural frequencies of the plates, thus the remodulations generate curves that are accurately aligned in frequency because the models are in complete similitude. The relevant information of these plots is not so much the overlap itself, which is expected, but the fact that the overlapping curves are reconstructed by noisy measurements and that, although polluted by uncertainties, they scale accordingly to the same scale factor. This implies that the input information is kept and it is not distorted.

For sake of completeness, the same procedure is carried out when the excitation frequency is equal to the second natural frequency. The results are shown in Fig. 4 and confirm the previous ones: the presence of noise leads to underestimated amplitudes, but the remodulation process still works fine.

Therefore, the outcomes exhibited in Figs. 3 and 4 demonstrate that the SOBI algorithm can extract the excitation signal from a set of noisy ones. On the one hand, the presence of noise affects the reconstruction of the force amplitude; on the other hand, the information extracted is coherent enough to follow the scaling procedure.

Equation (12) is then used to evaluate the velocity response. The mode shapes ϕ_{mn} are polluted with random Gaussian noise with three different values of standard deviation (1%, 5%, and 10%) to analyze the impact of uncertainties on the reconstruction of the frequency response. Also in this case, the final objective is to verify the overlap of velocity curves after the scaling procedure. According to equation (15), the velocity scale factor is $r_V = 0.5$.

Fig. 5 summarizes the results obtained at the first resonance frequency. When the level of noise is low, the remodulation is accurate (Fig. 5(a)). However, the more data becomes polluted, the more discrepancies in amplitude begin to appear (Fig. 5(b)), increasing significantly when the noise is high (Fig. 5(c)).

These outcomes are corroborated by applying the same procedure to the second mode, as shown in Fig. 6. The effect of noise pollution is clearly noticeable also in this case.

Table 3 Scale factors of the proportional sides model

Length, r_a	0.85
Width, r_b	0.85
Thickness, r_h	1.00
Mass, r_M	0.72
Natural frequency, r_ω	1.38
Velocity, r_V	1.01

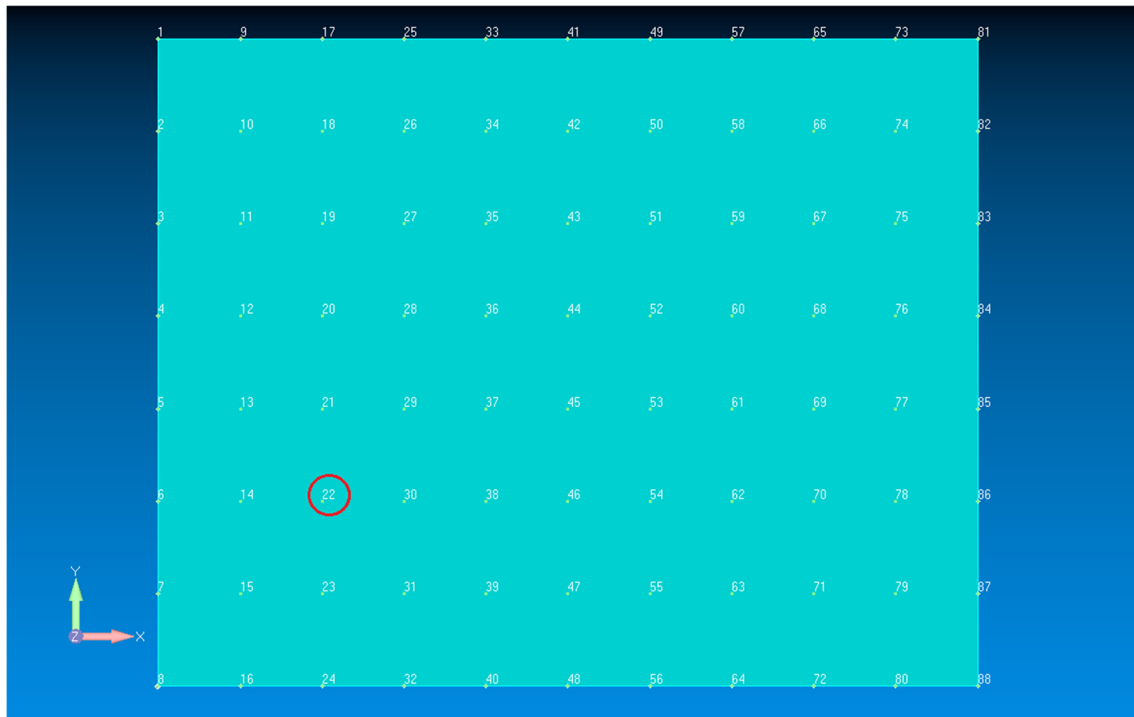


Fig. 2 Numerical mesh. The red circle indicates the excitation point

Thus, in comparison with the reconstruction of excitation force spectra, the presence of noise affects much more the evaluation of velocity response, impairing the scaling process if the uncertainty level is too high.

Experimental Setup

Two aluminium foam sandwich plates are tested with simply supported boundary conditions. Their geometrical characteristics and the masses are summarized in Table 4. The material properties of the skins are the same of those listed in Table 2, while Table 5 reports the core properties (provided by D'Alessandro et al. [14]) obtained by means of Ashby's laws. It is important to underline that the foam core is not homogeneous because of the random distribution of voids, which generates an inhomogeneous distribution of mass and stiffness. However, the material properties listed in Table 5 refer to the equivalent, uniform material having relative density equal to 0.222. Therefore, during the scaling procedure, the core is treated as an isotropic, homogeneous material, simply described by Young's modulus, mass density per unit volume and Poisson's ratio. The scale factors are summarized in Table 3 also for the sandwich plates.

Fig. 7 illustrates the experimental setup; the test articles are shown in Fig. 8. The displacements are captured by two high-speed synchronized cameras connected to DIC software, all corresponding to the Q450 high-speed DIC

system by Dantec Dynamics. The cameras have a maximum acquisition frequency of 7530 frames per second at a resolution of 1 MP; the displacement precision is of the order of 0.02 pixels. Each acquisition consists of 1000 samples. No averaging is adopted. The frequency range covers up to 31,400 rad/s (already considering Nyquist Theorem, therefore the bandwidth of interest is 0–15,700 rad/s). Arranging the DIC cameras in a stereoscopic configuration, each point of the plate is focused on a specific pixel in the image plane of each camera. By applying a stochastic texture to both prototype and proportional sides, the plates surfaces result as an indistinguishable intensity pattern to both cameras. The image of the first camera is subdivided into several subimages, called facets, used by a correlation algorithm which determines a suitable transformation of each facet, matching the homologous area in the second camera image. Executing this procedure for every loading step of the object under test, it is possible to follow the facet deformation during all the experiment [32, 33].

The excitation waveform is given by means of a signal generator, linked to an amplifier and an electrodynamic shaker which excites the plate.

The points of measurement are determined by overlapping a virtual grid to the image of the test article, contained into a frame, called mask, which separates the specimen from the background and indicating which part of the field of view must undergo the measurement procedure. The

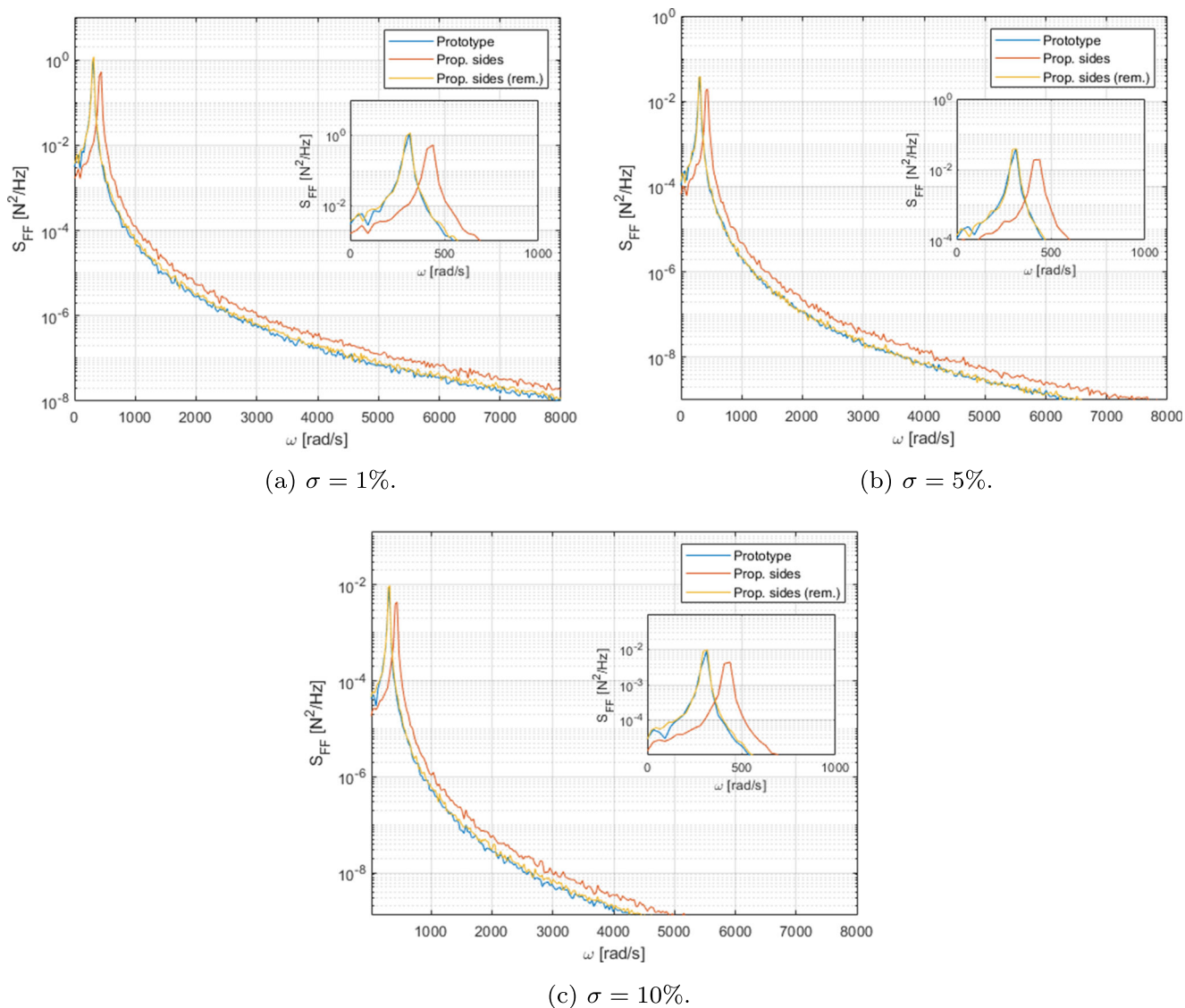


Fig. 3 Remodulation of the spatially averaged force PSD, first natural frequency (P: 303.45 rad/s; PS: 424.59 rad/s); noise standard deviation equal to 1% (a), 5% (b), and 10% (c)

dimensions of the grid points and facets are determined on the basis of a trade-off among several matters [5, 33].

Firstly, the more dense the grid is, the better is the spatial representation of the variable under investigation (the displacement, in this case); however, this would imply more grid points to process, therefore an increasing computational effort and memory space are required. Reducing the number of points would ease the computational and memory burden, at the cost of a more coarse spatial description of the displacements.

Then, the statistical error previously introduced is directly linked to the facet size. In fact, as the facet dimension increases, this error reduces with the square root of the number of facet pixels. However, the results of the measurement are evaluated as mean values for each facet. Thus,

increasing their dimension leads to a decrease of spatial resolution, too.

Taking into account these aspects, the resulting trade-off leads to choose, for both prototype and proportional sides model, a virtual grid made of 30x44 square elements, with a total of 1345 grid points. The dimensions of the grid element and the facet of the prototype are, respectively, 20x20 and 23x23. Being fundamental to compare the displacements of homologous points, the grid spacing of the proportional sides is scaled down with scale factor 0.85 (that is, the same of length and width of the plate), so that the grid elements have dimensions 17x17. The facet is set to 21x21.

The simply supported plates are excited in one point, having nondimensional coordinates (0.2000, 0.2875), with a sinusoidal force at a specific frequency (for each natural

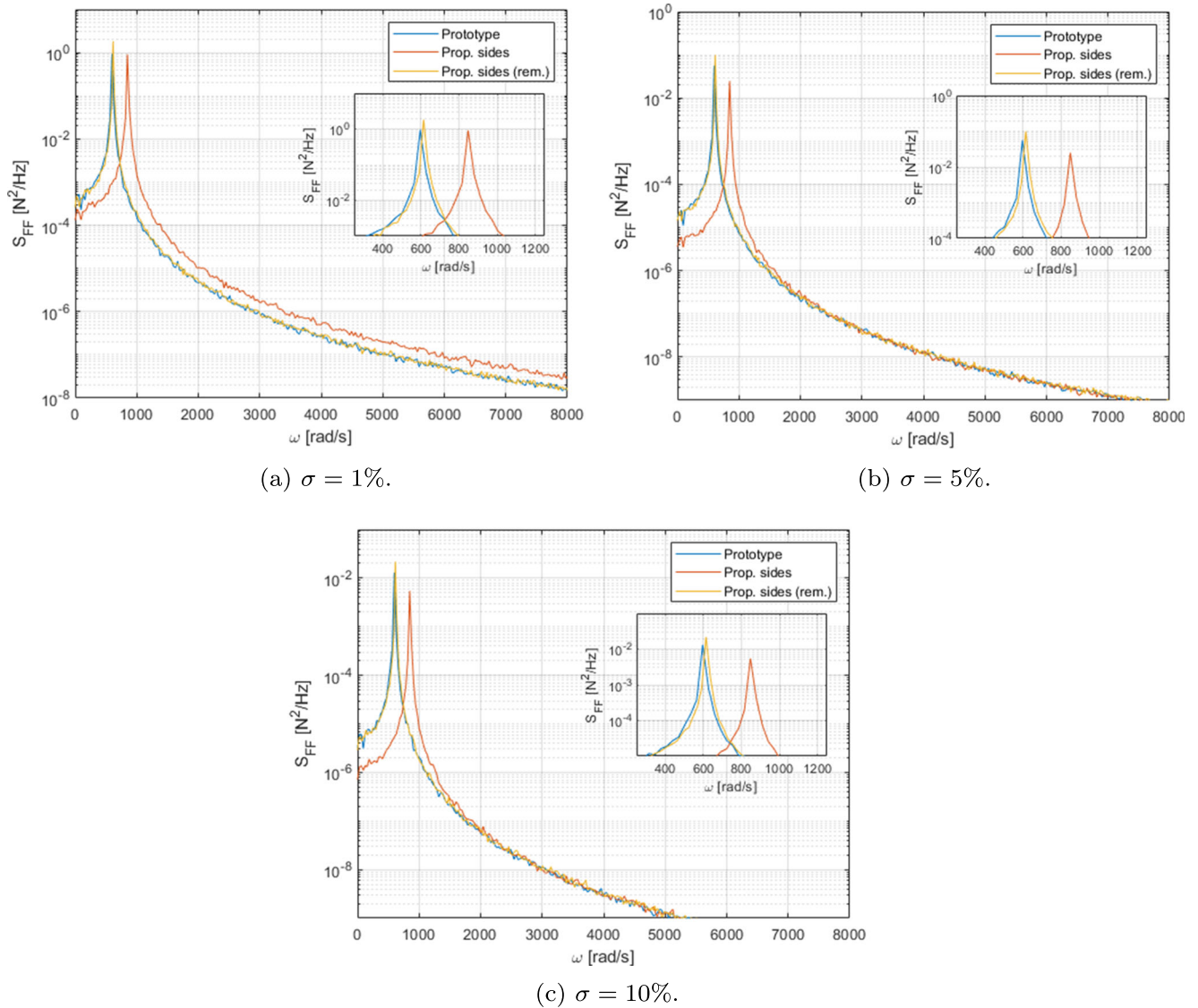


Fig. 4 Remodulation of the spatially averaged force PSD, second natural frequency (P: 602.88 rad/s; PS: 852.89 rad/s); noise standard deviation equal to 1% (a), 5% (b), and 10% (c)

frequency of the plate previously evaluated by an experimental modal analysis). The prototype and proportional sides are excited with the same waveform but with different and unquantified amplifier gain.

Fig. 9 gives an example of the measured displacement. The plot shows a noticeable noise. This can be due not only to the contactless characteristic of the measurement procedure itself, but also to the precision of the DIC cameras. In fact, the sandwich panels are characterized by an high stiffness-to-weight ratio, and the simply supported boundary conditions adds an artificial stiffness. Moreover, the displacement amplitude of each point decreases as the modal order increases. All these elements lead to very small displacements with values assessing below the DIC camera precision, especially when frequency increases. Adding

to all these contributions the sources of statistical errors previously described, leads to results with a noticeable level of noise. Therefore, for this test it is not possible to use the measurements as they are carried out but they needed post-processing.

Reconstruction of Excitation Spectra

With the exception of the sinusoidal waveform, no other information is known about the force in terms of amplitude, being the gain of the amplifier unknown. Therefore, the SOBI algorithm is used to determine the spectra of the input forces. The results in “Numerical Plates” demonstrate that the input information, contained into the measured displacement time histories, is kept and such

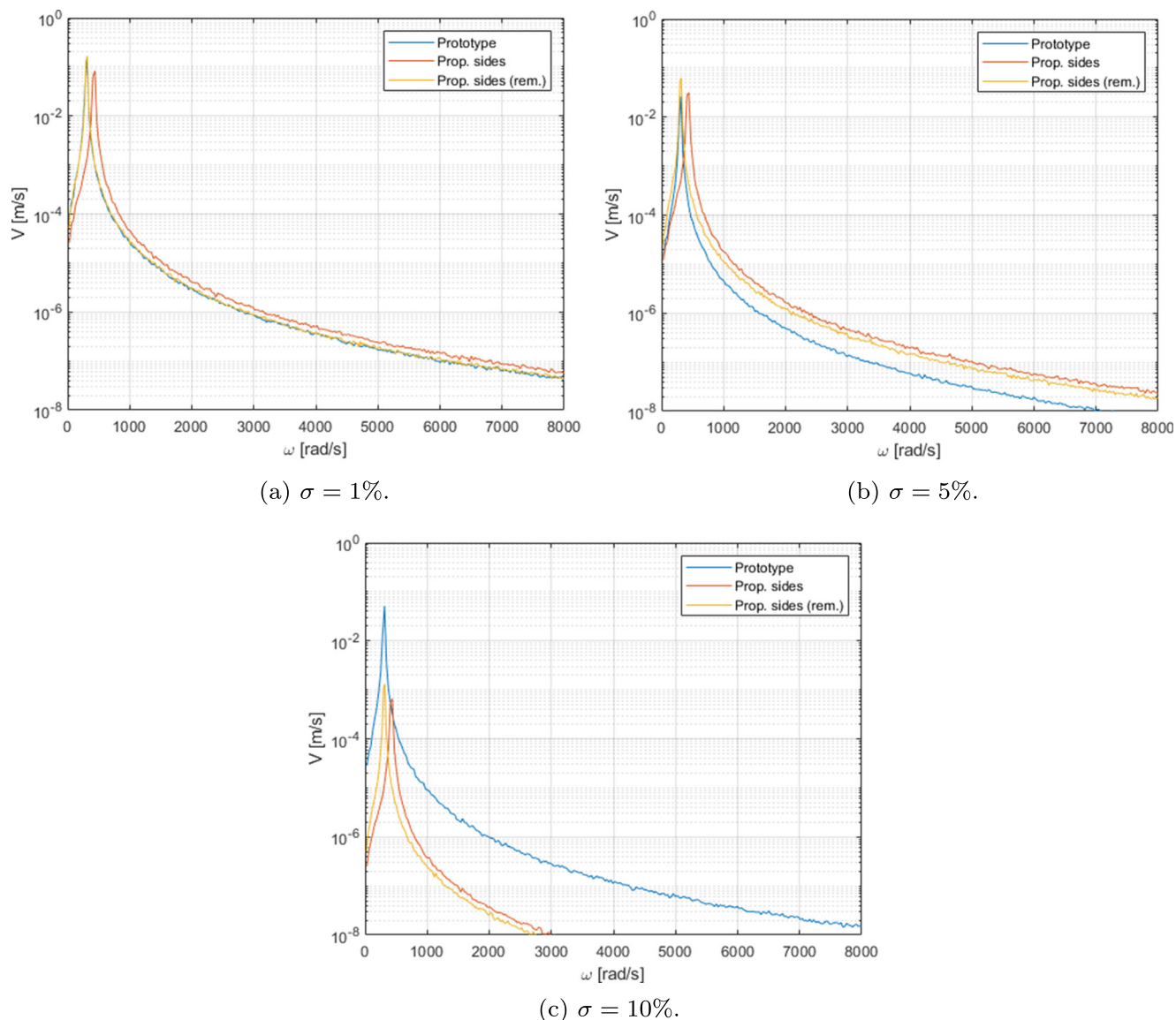


Fig. 5 Remodulation of the spatially averaged velocity, first natural frequency (P: 303.45 rad/s; PS: 424.59 rad/s); noise standard deviation equal to 1% (a), 5% (b), and 10% (c)

an information is coherent enough to follow the scaling procedure. Therefore, it would be possible, as a rule of thumb, to derive the scale factor of both force PSD and amplitude by overlapping the curve of the prototype and the curve of the model (after frequency remodulation).

Always with reference to the list in “[Similitude Method](#)”, this time the experimental structural responses required in step 1 are provided by the DIC measurements. The structural loss factor is set to 0.02.

The spatially averaged PSD of the excitation force (and the zoom on the peaks) is shown in Fig. 10 for the first three excitation frequencies. The proportional sides curves (the red ones) are first remodulated only in frequency, so that the values of force PSD could be compared at homologous

points in frequency and determine the scale factor. For this purpose, 30 points are selected for each curve (mainly clustered around the resonance peak), then the scale factor for each point is evaluated. The mean value, obtained by averaging on all the points and all the excitation frequencies, of force PSD scale factor is $r_{SF} = 0.67$, which returns very good amplitude scaling, as the remodulated (yellow) curves illustrate.

The results of Fig. 10 show that the SOBI algorithm is still capable of returning coherent information about the excitation even though the sources of experimental uncertainties.

The inhomogeneity of the foam leads to slight discrepancies in frequency between the prototype and the model

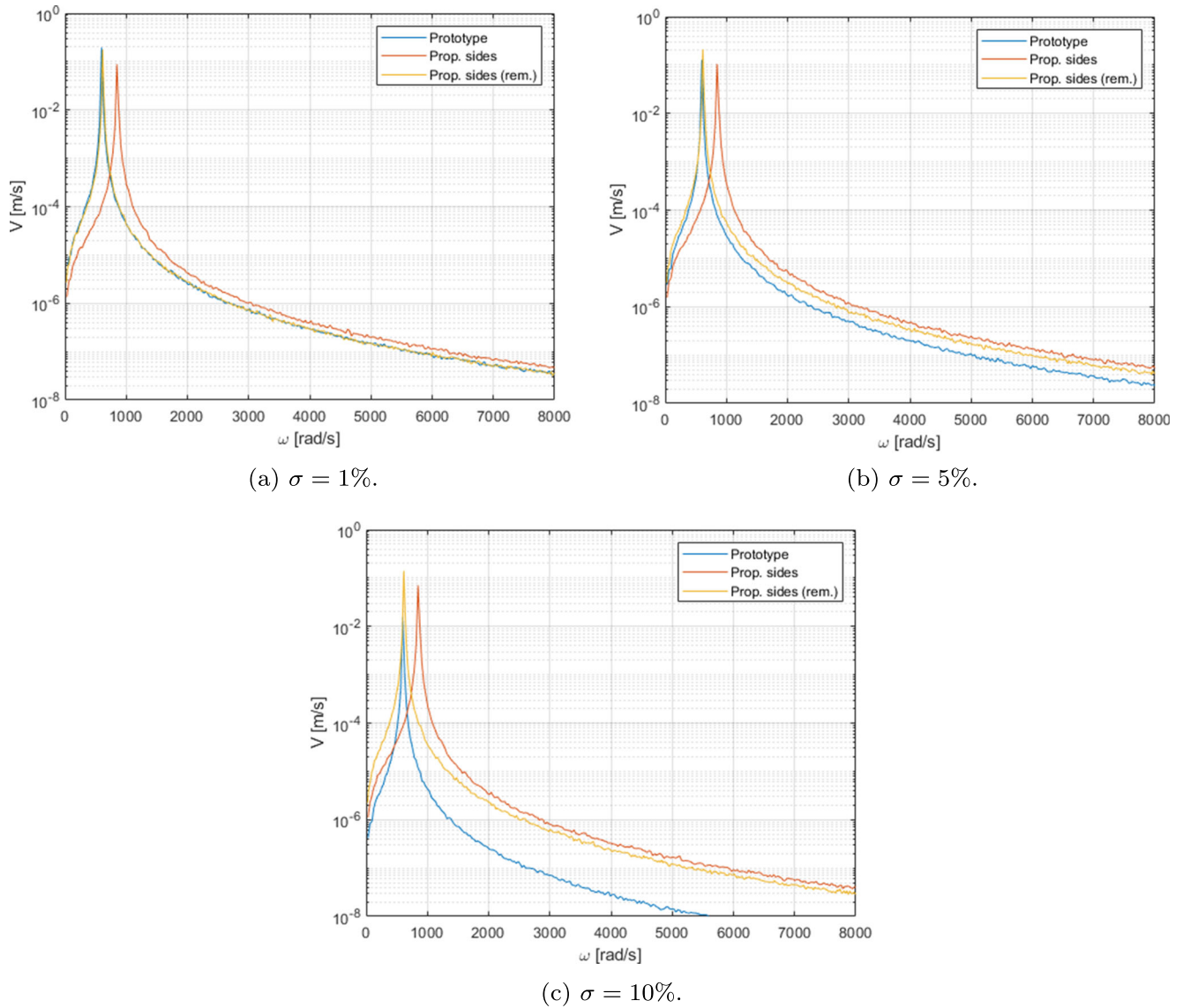


Fig. 6 Remodulation of the spatially averaged velocity, second natural frequency (P: 602.88 rad/s; PS: 852.89 rad/s); noise standard deviation equal to 1% (a), 5% (b), and 10% (c)

remodulated curve. These discrepancies are noticeable since the fourth resonance. For this reason, the force scale factor is evaluated considering only the first three modes shown in Fig. 10. In fact, the missing overlap would have prevented the direct comparison of homologous points in frequency. Furthermore, it will be illustrated further that these modes

are the only ones well identified for both prototype and proportional sides, therefore they are considered as the most reliable for extracting the input scaling characteristics.

Fig 10 also shows that the amplitude of the PSDs decreases in frequency, even though the excitation amplitude is the same for each model. A likely reason may lie

Table 4 Geometrical characteristics and mass of the prototype and proportional sides sandwich plates

	a [m]	b [m]	t_f [m]	t_c [m]	M [kg]
P	0.656	0.476	0.001	0.008	3.2
PS	0.558	0.405	0.001	0.008	2.34

Table 5 Aluminium foam core material properties

Young's modulus, E_c	6.48 GPa
Mass density, ρ_c	600 kg/m ³
Poisson's ratio, ν	0.31
Relative density, ρ_r	0.222

Fig. 7 Experimental setup



into the decreasing value of displacements, when moving to further modes, which become less recognizable to the DIC cameras.

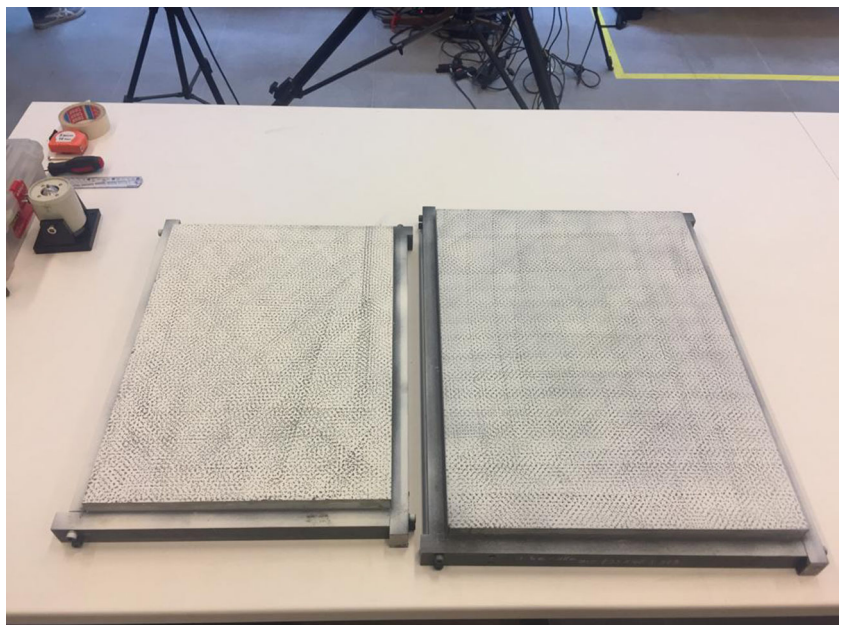
Reconstruction of Velocity Response

The force spectra determined in the previous section are reliable enough to be used in equation (12) and reconstruct, analytically, the velocity response. All the parameters in this equation are known: modal mass (equation (13)), natural frequencies, and the mode shapes ϕ_{mn} , the latter provided by DIC measurements in terms of displacement field.

From the force PSD scale factor, the force amplitude scale factor $r_F = 0.82$ is deduced. This value is inserted into equation (15), which returns a velocity scale factor $r_V = 0.81$. This is the velocity amplitude scale factor needed to scale the velocity response of the proportional sides back to that of the prototype.

Fig 11 shows the displacement fields of both prototype (Fig. 11(a)) and proportional sides (Fig. 11(b)), and the reconstruction and remodulation of the velocity curves (Fig. 11(c)). Both the displacement fields give a good representation of the first mode shape. Inserting the normalized values of these displacements into equation (12)

Fig. 8 Experimental plates with speckle patterns for DIC analysis



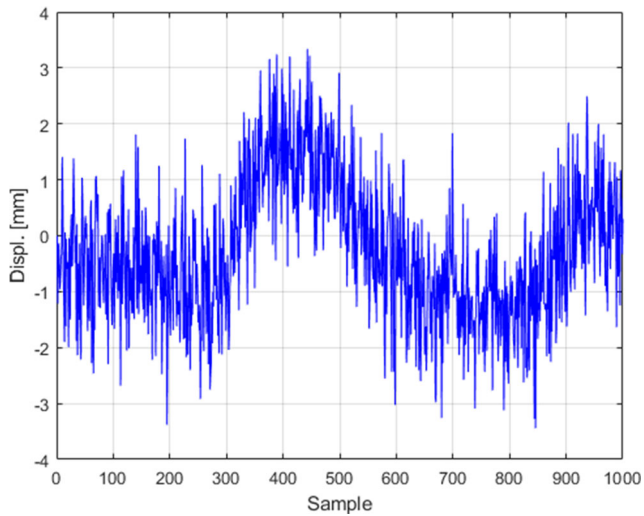
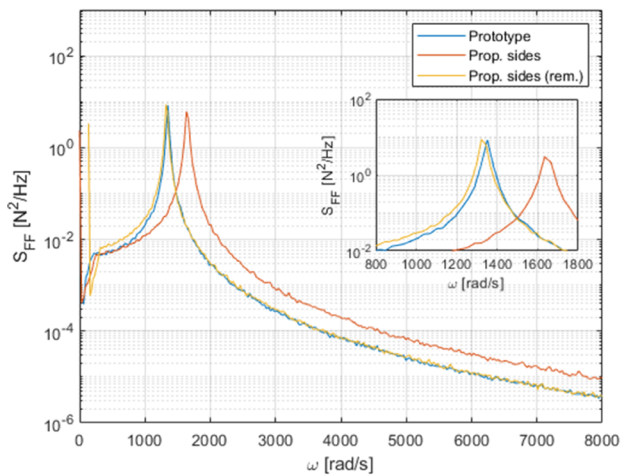


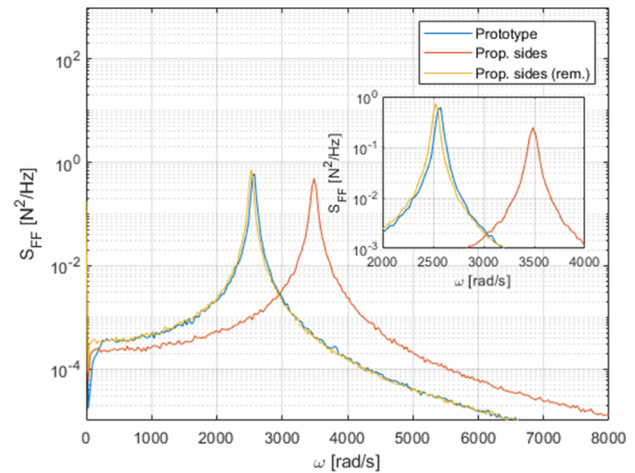
Fig. 9 Prototype displacement of point no. 100, mode 1 (1350 rad/s)

leads to the velocity curves of Fig. 11(c), that can be read as the force curves previously showed. As before, the frequency remodulation is a consequence of SAMSARA that does not give any information on the experimental result. What is important, instead, is the amplitude level of the prototype, which is reconstructed accurately. This happens because the mode shapes are not only well reconstructed, but also because the normalized values of displacements are coherent between the prototype and the proportional sides. Therefore, just by looking at the velocity curves, one may say that the experimental information is reliable and that the measurement is executed successfully.

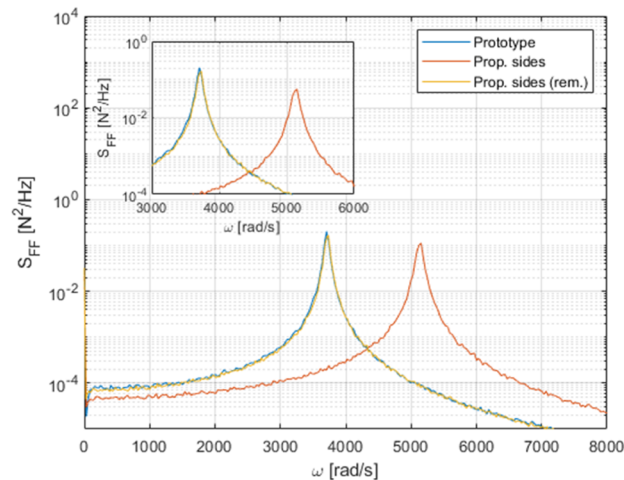
These conclusions are strengthened by the results obtained with the second mode, and shown in Fig. 12. The remodulated curve matches accurately the prototype curve (Fig.12(c)) in amplitude. Again, this happens because the mode shapes of the prototype (Fig. 12(a)) and proportional



(a) Mode 1 (P: 1350 rad/s; PS: 1645 rad/s).



(b) Mode 2 (P: 2562 rad/s; PS: 3485 rad/s).



(c) Mode 3 (P: 3705 rad/s; PS: 5130 rad/s).

Fig. 10 Remodulation of the force PSD for mode 1 (a), 2 (b), and 3 (c)



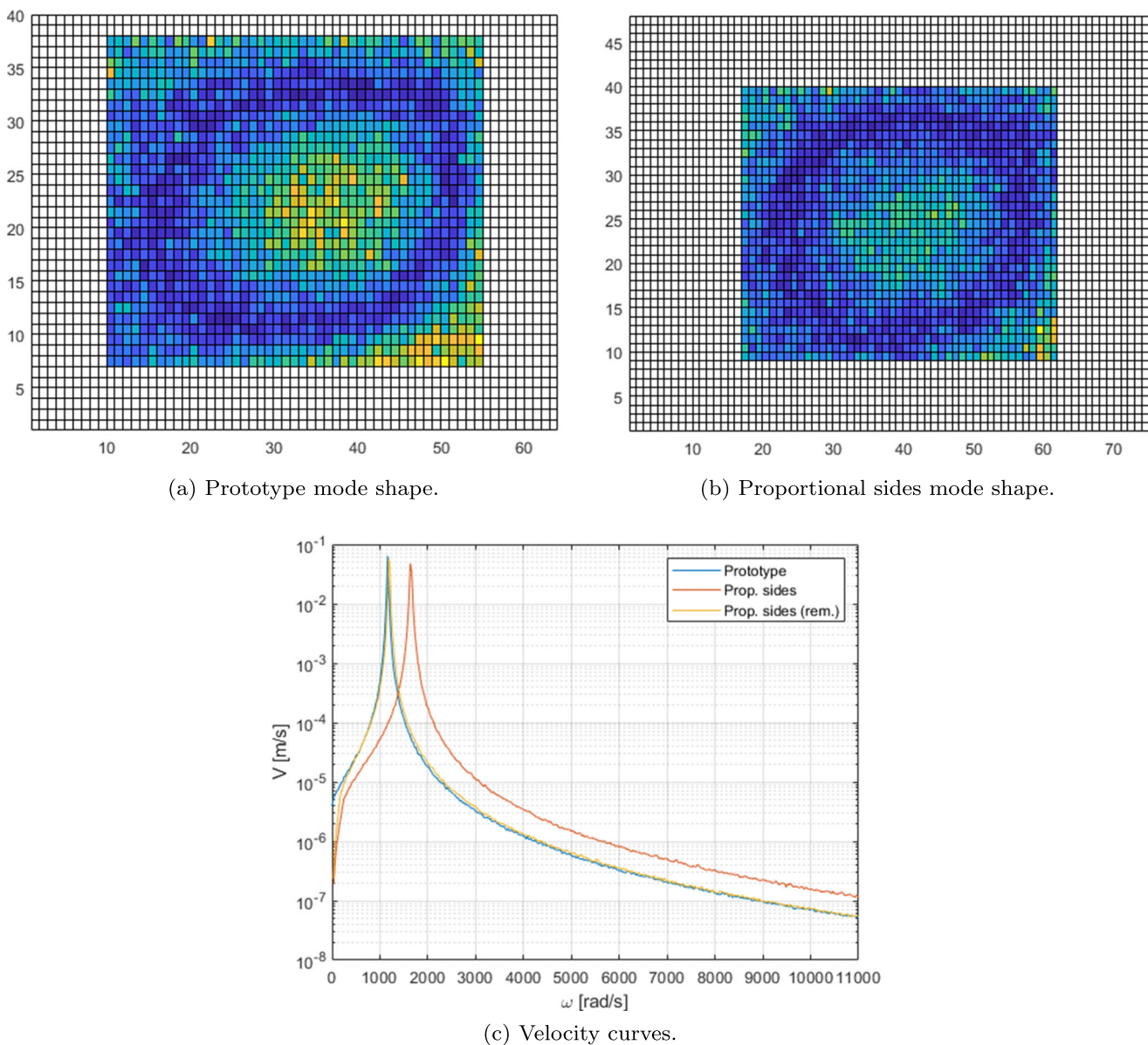


Fig. 11 Mode shapes and velocity remodulation of the first mode (P: 1350 rad/s; PS: 1645 rad/s)

sides (Fig. 12(b)) not only are still recognizable, but also the normalized values of local displacements are coherent.

The amplitude remodulation shows some discrepancies when the modes begin to be less recognizable, like in the case of the fourth mode. In fact, while the prototype mode shape (Fig. 13(a)) is quite clear, the proportional sides one is not (Fig. 13(b)), except for the right side of the displacement map, which exhibits some peak values that may be associated with the right lobe of the mode. However, the scaling procedure highlights the lack of an identifiable spatial pattern and the consequent absence of coherence between the local displacements.

About the frequency remodulation, it is noticeable a slight shift of the resonance peaks. As previously specified, this phenomenon is independent of the quality of the measurements and the similitude method. It is due to the inhomogeneous distribution of mass and stiffness of the foam core.

The results are more dramatic when the mode shapes are not identified at all. An example of this case is the sixth mode, shown in Fig. 14. The velocity values of the scaled curves (Fig. 14(c)) are totally different, more than one order of magnitude, as the mode shapes of both prototype (Fig. 14(a)) and proportional sides (Fig. 14(b)) are not

Fig. 12 Mode shapes and velocity remodulation of the second mode (P: 2562 rad/s; PS: 3845 rad/s)

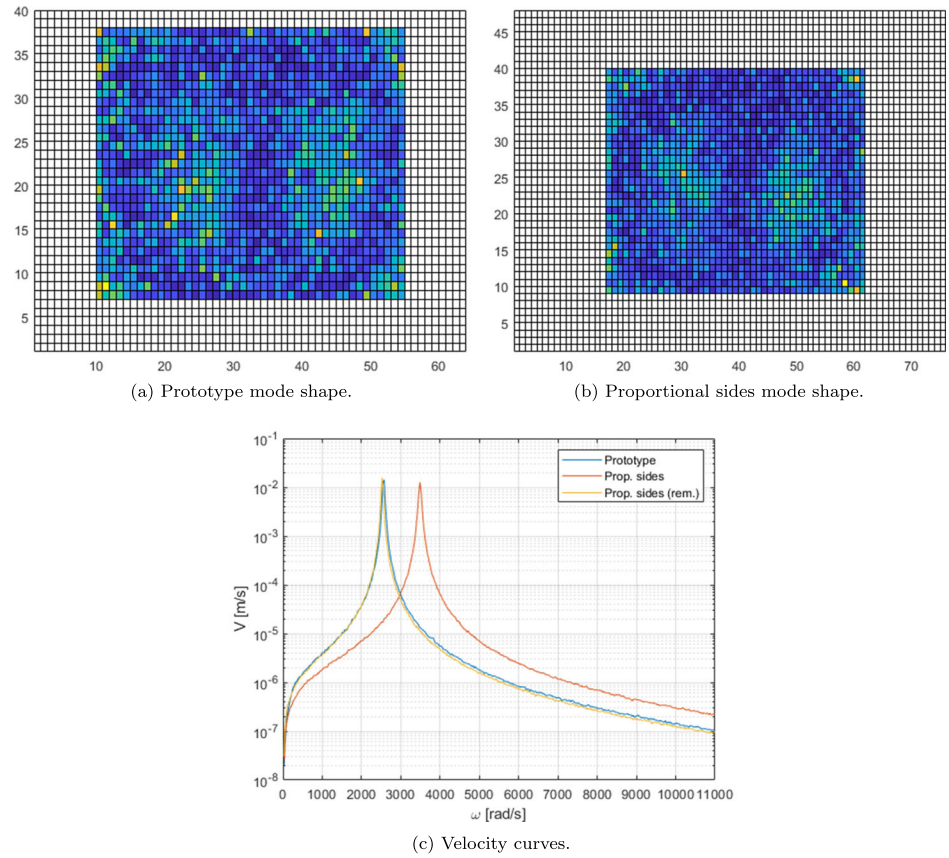
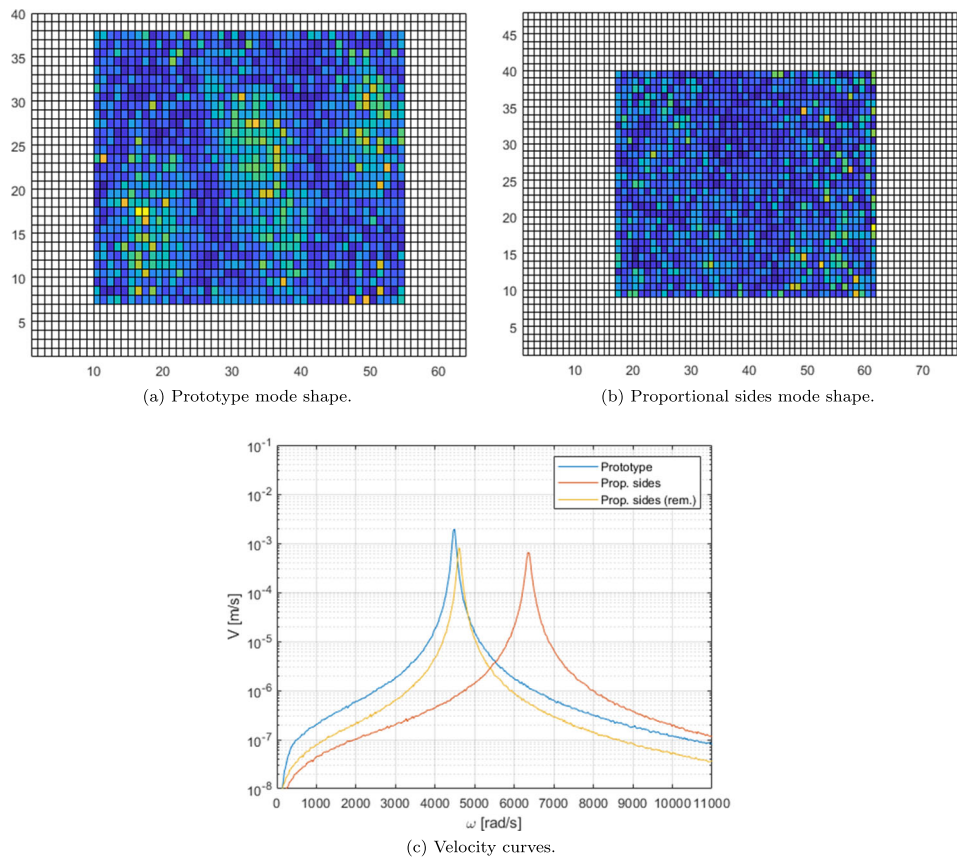


Fig. 13 Mode shapes and velocity remodulation of the fourth mode (P: 4477 rad/s; PS: 6355 rad/s)



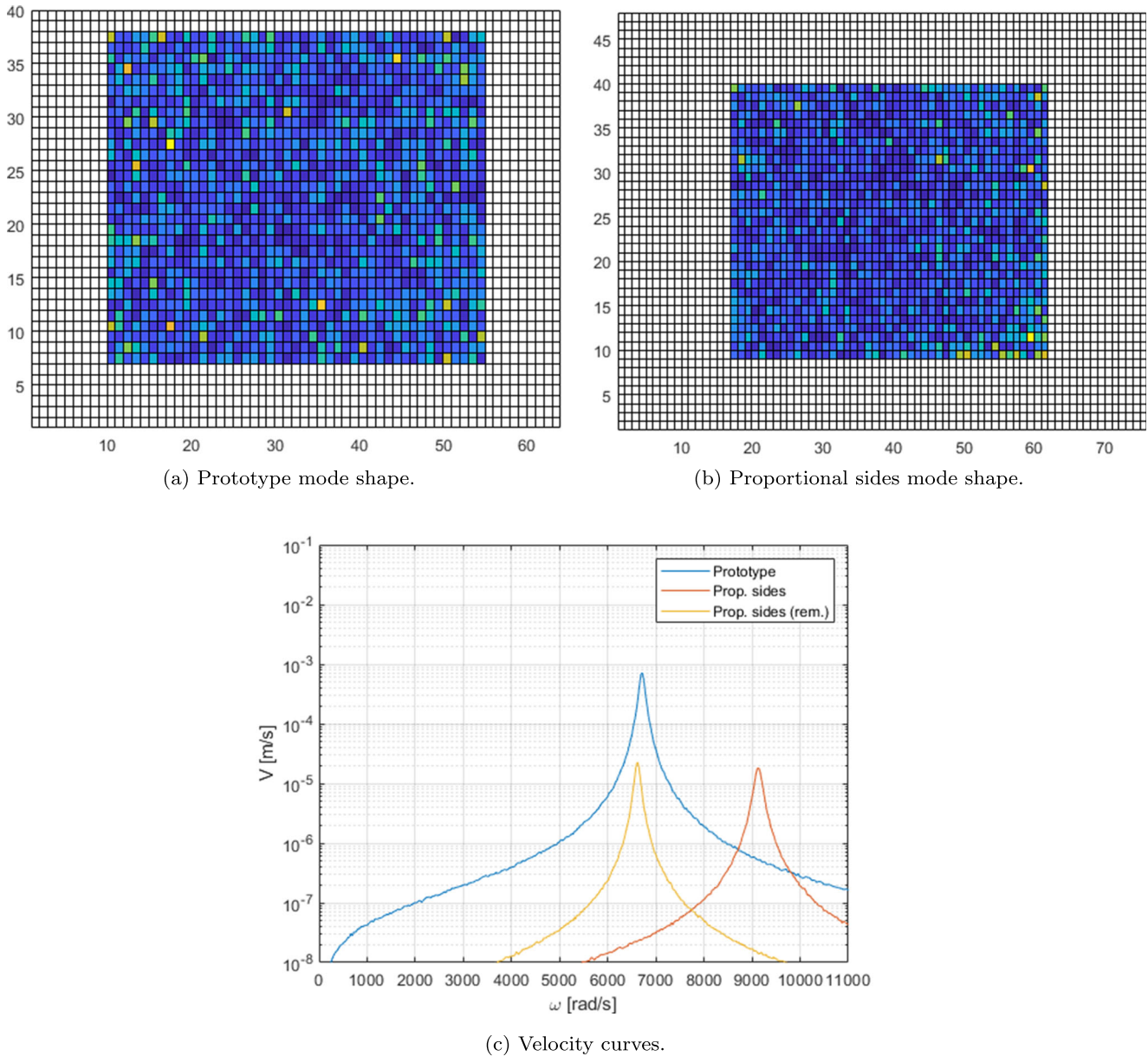


Fig. 14 Mode shapes and velocity remodulation of the sixth mode (P: 6707 rad/s; PS: 9124 rad/s)

identified at all. The plate displacements become smaller as the frequency increases, confusing with the noise. Thus, the displacement field exhibits totally uncorrelated values.

These results prove that, provided a reference test article - the prototype - which behavior is known, if a model fulfilling the similitude conditions is tested, then the similitude theory helps to understand the quality of an experiment polluted by noise and to validate it.

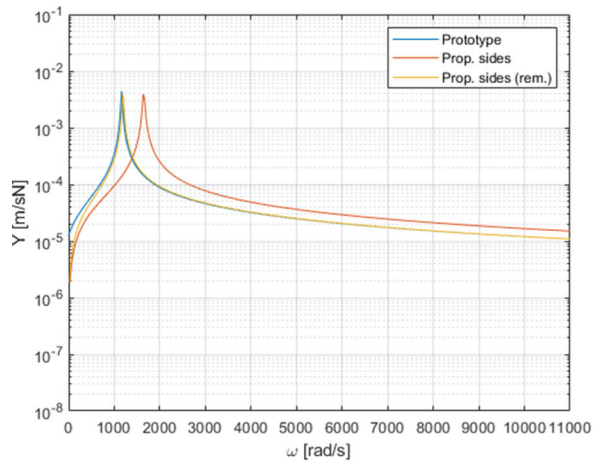
Reconstruction of Mobility

As done with the velocity, the mobility can be reconstructed analogously with equation (16), according to which the

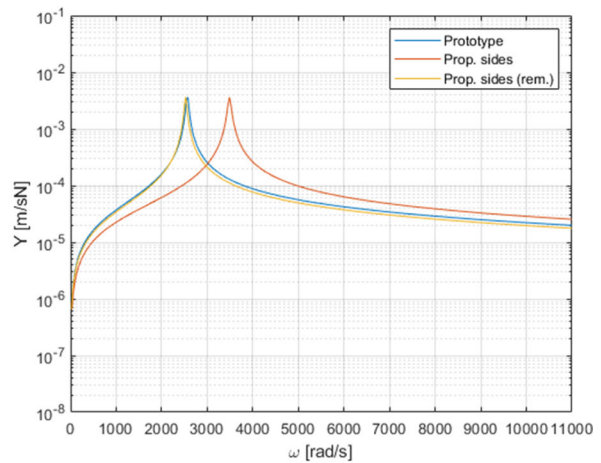
mobility scale factor is $r_Y = 0.99$. In this way, the dynamic response of the plates is derived without directly involving the force spectra obtained with the SOBI algorithm.

Fig. 15 gathers the curve remodulations of the same modes previously examined. All the plots confirm the results shown up to now: the similitude is able to indicate which modes are well reconstructed and which not.

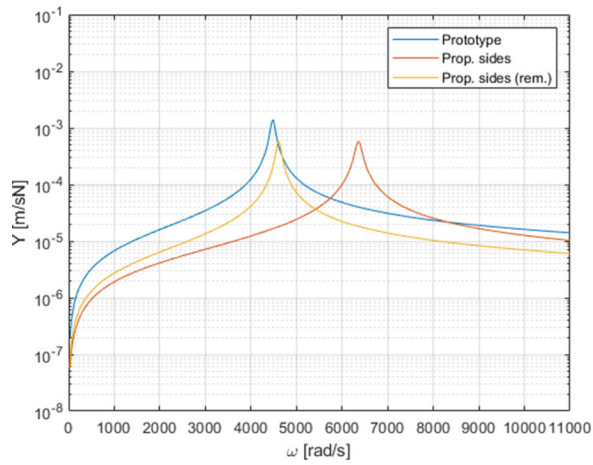
The curves in Fig. 15 may appear as a simple repositioning of those in Figs. 10, 11, 12 and 13, however they can be overlapped to the results of the experimental campaign made with accelerometric measurements and check the quality of the data post-processed from DIC measurements. The results are shown in Fig. 16(a)–(b).



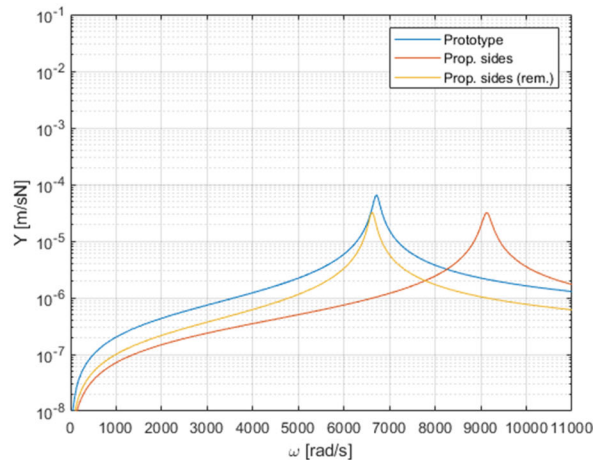
(a) Mode 1 (P: 1350 rad/s; PS: 1645 rad/s).



(b) Mode 2 (P: 2562 rad/s; PS: 3845 rad/s).

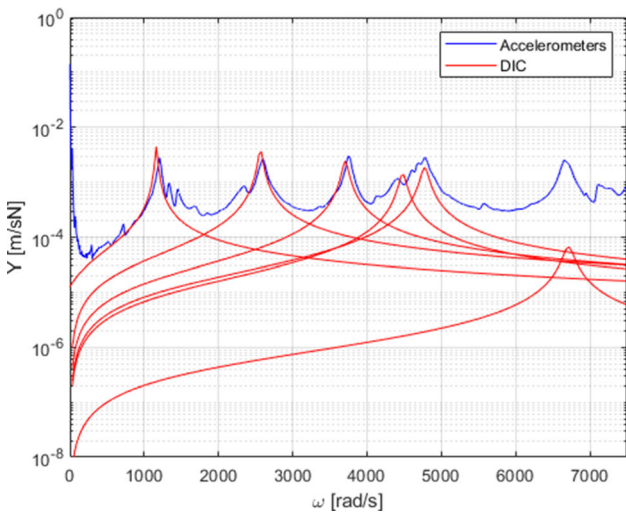


(c) Mode 4 (P: 4477 rad/s; PS: 6355 rad/s).

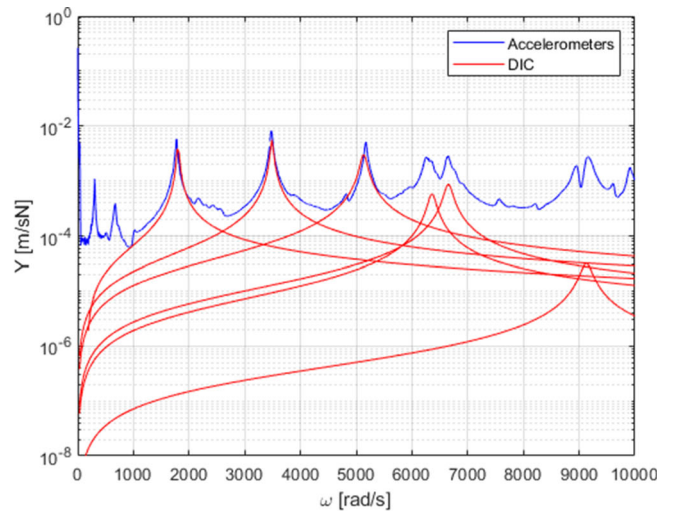


(d) Mode 6 (P: 6707 rad/s; PS: 9124 rad/s).

Fig. 15 Mobility remodulation curves of the first (a), second (b), fourth (c), and sixth (d) mode



(a) Prototype.



(b) Proportional sides.

Fig. 16 Comparisons between the accelerometric and DIC measurements of spatially averaged mobility

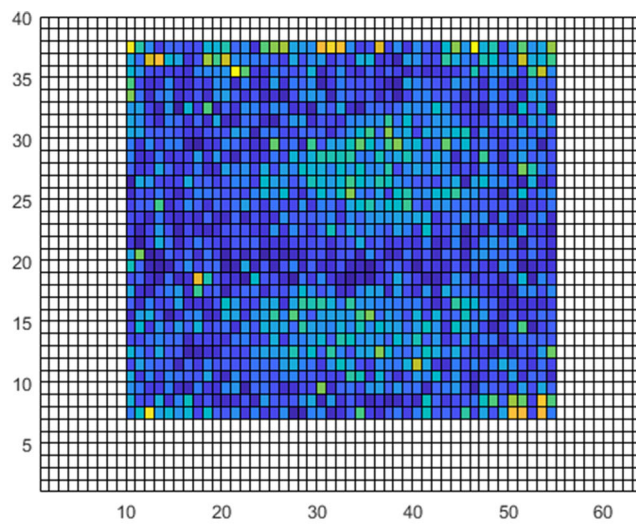


With reference to Fig. 17, which illustrate the experimental displacement field of the third and fifth modes (not yet shown until now), the prototype curves in Fig. 16(a) exhibit a very good match between the accelerometric and DIC measurements. The first five modes are well predicted, as the spatial patterns are reasonably reconstructed (Fig. 17(a)–(b)), and this is in agreement with the fact that these mode shapes are well recognized by DIC cameras. The sixth mode, instead, is not well identified, and the mobility evaluation leads to a seriously underestimated resonance peak.

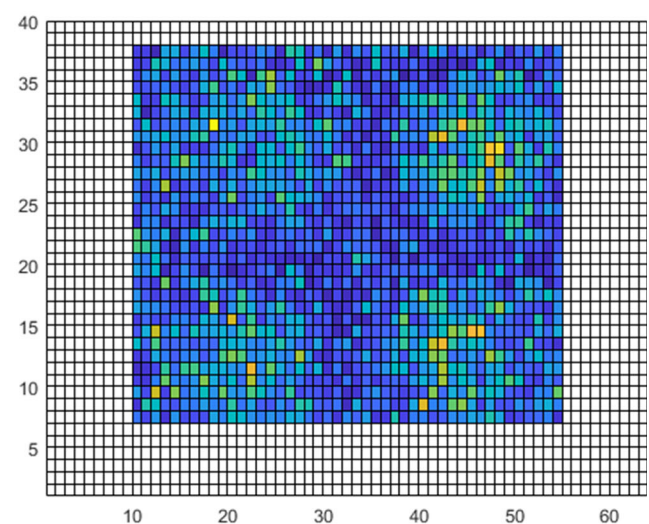
These considerations are validated by the comparisons between the accelerometric and DIC measurements of the proportional sides (Fig. 16(b)). The good evaluation of the first three resonance peaks is in agreement with the

identification of the associated mode shapes. From the fourth mode on, instead, the peaks are underestimated.

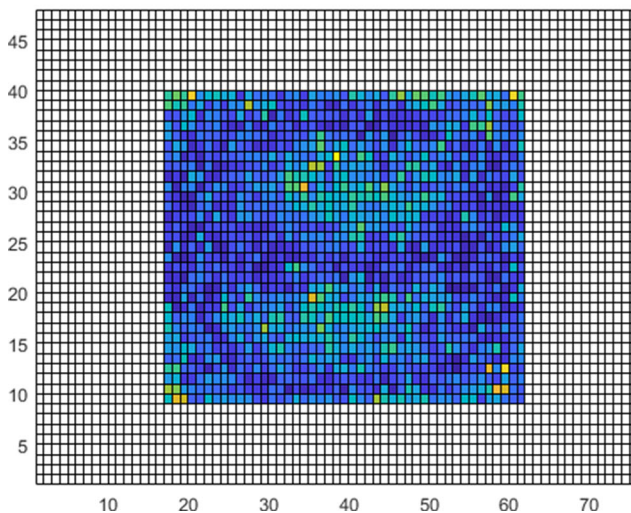
For sake of completeness, the correlation between the experimental mode shapes of prototype and proportional sides is shown in Fig. 18, which displays the Modal Assurance Criterion (MAC) ([18]). The bars reported confirm the results obtained. The first modes of prototype and proportional sides exhibit the higher correlation, upholding that the DIC system captures this mode satisfactorily. The second and third mode shapes follow in order of decreasing correlation, since the cameras roughly identify the form of the mode, but noise becomes noticeable. There is no correlation between the fourth, fifth and sixth modes because, even though some shapes are well identified in one model (for example, the fourth and fifth



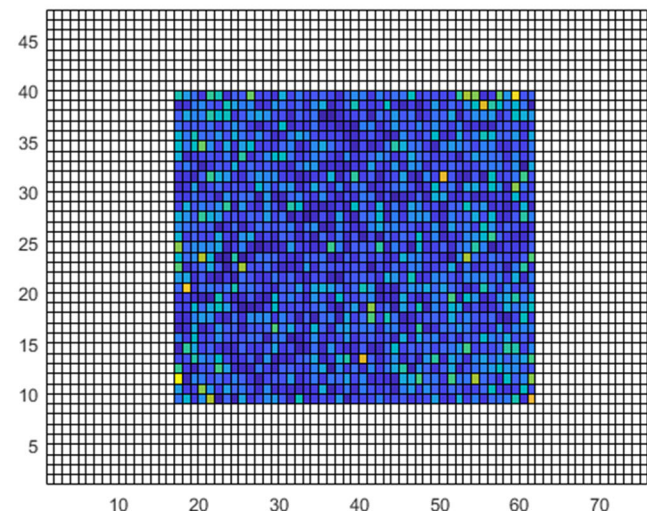
(a) Prototype mode 3, 3705 rad/s.



(b) Prototype mode 5, 4772 rad/s.



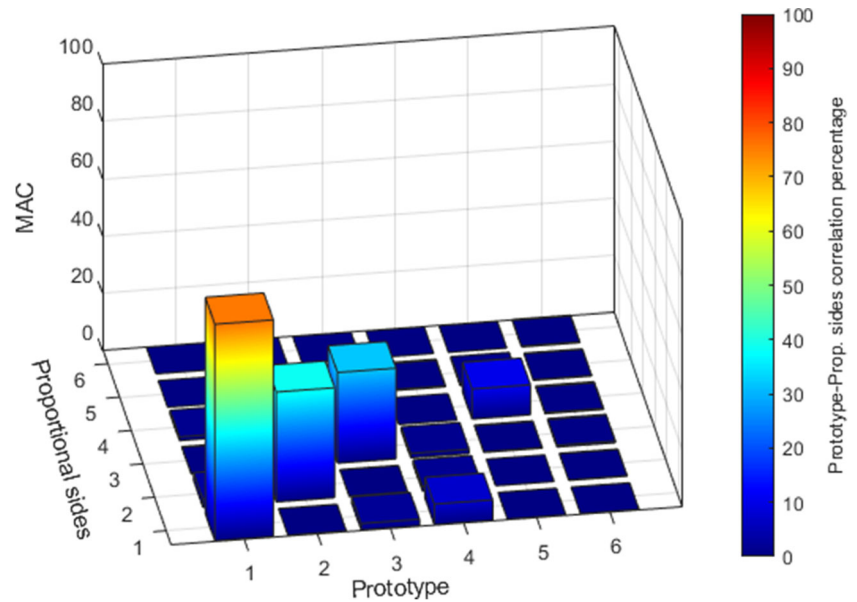
(c) Proportional sides mode 3, 5130 rad/s.



(d) Proportional sides mode 5, 6650 rad/s.

Fig. 17 Spatial patterns of the third and fifth mode shapes of both prototype and proportional sides

Fig. 18 MAC between the experimental mode shapes of prototype and proportional sides



modes of the prototype), they are not in the other. The remaining comparisons return MAC values equal to zero, except for the 4th-1st and 5th-4th couples of prototype and proportional sides. However, these values of correlation are comprised about in the range 10%-0%, and can be considered as outcomes due to noise.

Conclusions and Further Research

This work has dealt with the investigation of similitude methods as a mean to support noisy experimental measurements. For this purpose, the dynamic response of two AFS plates in complete similitude is observed with two DIC cameras. As the measured data is strongly polluted by noise, the response must be reconstructed analytically, using the displacement field as experimental data.

Firstly, the time response of each point is used as input for a SOBI algorithm which returns the spectra of the input excitations. In this way, it is possible to:

1. reconstruct the input information,
2. check whether such an information is coherent, and
3. evaluate a unique force scale factor, needed for the velocity response.

Then, by remodulating the velocity response for each mode, it is demonstrated that the curves overlapped accurately when the DIC measurements are able to recognize the spatial pattern in resonance. When the mode of just one of the models is not well identified, then the remodulation exhibits noticeable discrepancies.

These results are obtained also by considering the mobility, which is then overlapped to accelerometric measurements to demonstrate that the analytical reconstruction is consistent. Of course, the comparison between accelerometric and DIC measurements is acceptable only for the resonances corresponding to the identified modes. In the other cases, the peak values are seriously underestimated.

In conclusion, it is demonstrated that the similitude results are coherent with the quality of the experimental measurements, and the comparison between the accelerometric and DIC measurements show that the analytical reconstruction, on which the remodulation is based, are consistent. Therefore, similitude methods reveal to be an interesting tool for understanding if a set of measurements is reliable or not, especially in the light of an expanding range of approaches (classical modal analysis, but also machine learning techniques for noisy or missing data, as well as the SOBI algorithm herein used) which allow to extrapolate important information from observations polluted by random uncertainties, as expected.

Up to now, the main obstacle which may prevent a wider application of similitude as validation tool is that the model must be in complete similitude. Thus, more research should be dedicated to similitude methods and the way in which the similitude conditions are derived, in order to reduce the range of possible distorted models. The scaling procedures involving the structural wavenumber, representative of the mode shape, seems to be a promising direction. In fact, it would allow to consider one mode at time, instead of the whole succession of modes, which would also fit the single-mode approach with DIC cameras herein used.

Acknowledgements The research investigation reported in this paper was carried out during the secondment at Universidad de Chile, in Santiago de Chile, of dr. Alessandro Casaburo and Dr. Giuseppe Petrone. The secondment of Dr. Petrone was funded by MIUR (Ministero dell'Istruzione, dell'Università e della Ricerca) and CRUI (Conferenza dei Rettori delle Università Italiane), since Dr. Petrone was winner in 2019 of the “Leonardo Da Vinci” award, task 2 “Mobility of young researchers”, in the MAECI-MIUR framework 2017/2020. All the authors would like sincerely to acknowledge MIUR and CRUI for this opportunity. Moreover, dr. Casaburo and dr. Petrone would like to acknowledge the University of Chile for the hospitality and willingness.

Author Contributions Alessandro Casaburo: Conceptualization, Methodology, Investigation, Validation, Software, Writing–Original Draft

Giuseppe Petrone: Conceptualization, Methodology, Investigation, Validation

Viviana Meruane: Investigation, Validation, Resources

Francesco Franco: Supervision, Conceptualization, Writing–Review & Editing

Sergio De Rosa: Supervision, Conceptualization, Writing–Review & Editing

Funding Open access funding provided by Università degli Studi di Napoli Federico II within the CRUI-CARE Agreement.

Declarations

Conflict of Interests All authors certify that they have no affiliations with or involvement in any organization or entity with any financial interest or non-financial interest in the subject matter or materials discussed in this manuscript.

Open Access This article is licensed under a Creative Commons Attribution 4.0 International License, which permits use, sharing, adaptation, distribution and reproduction in any medium or format, as long as you give appropriate credit to the original author(s) and the source, provide a link to the Creative Commons licence, and indicate if changes were made. The images or other third party material in this article are included in the article's Creative Commons licence, unless indicated otherwise in a credit line to the material. If material is not included in the article's Creative Commons licence and your intended use is not permitted by statutory regulation or exceeds the permitted use, you will need to obtain permission directly from the copyright holder. To view a copy of this licence, visit <http://creativecommons.org/licenses/by/4.0/>.

References

- Adams C, Bös J, Slomski EM, Melz T (2018) Scaling laws obtained from a sensitivity analysis and applied to thin vibrating structures. *Mech Syst Signal Process* 110:590–610
- Asl M, Niezrecki C, Sherwood J, Avitabile P (2016) Similitude analysis of the strain field for loaded composite I-beams emulating wind turbine blades
- Asl ME, Niezrecki C, Sherwood J, Avitabile P (2017) Similitude analysis of the frequency response function for scaled structures. In: Barthorpe R, Platz R, Lopez I, Moaveni B, Papadimitriou C (eds) *Model validation and uncertainty quantification*, vol 3. conference proceedings of the society for experimental mechanics series. Springer, Cham
- Asl ME, Niezrecki C, Sherwood J, Avitabile P (2017) Vibration prediction of thin-walled composite I-beams using scaled models. *Thin-Walled Struct* 113:151–161
- Becker T, Splithof K, Siebert T, Kletting P (2006) Error estimations of 3D digital image correlation measurements. *Proc SPIE*, 6341:63410F–1–63410F–6
- Belouchrani A, Abed-Meraim K, Cardoso J, Moulines E (1997) A blind source separation technique using second-order statistics. *IEEE Trans Signal Process* 45(2):434–444
- Blevins RD (2016) *Formulas for dynamics, acoustics and vibration*. In: *The atrium, southern gate, chichester, west sussex*, PO19 8SQ. Wiley, United Kingdom
- Casaburo A, Petrone G, Franco F, De Rosa S (2019) A review of similitude methods for structural engineering. *Appl Mech Rev* 71(3)
- Casaburo A, Petrone G, Meruane V, Franco F, De Rosa S (2019) Prediction of the dynamic behavior of beams in similitude using machine learning methods. *Aerotecnica Missili e Spazio* 98(4):283–291
- Chen Y, Avitabile P, Dodson J (2020) Data consistency assessment function (dcdf). *Mech Syst Signal Process* 141
- Chen Y, Logan P, Avitabile P, Dodson J (2019) Non-model based expansion from limited points to augmented set of points using chebyshev polynomials. *Exp Tech* 43(5):521–543
- Coutinho CP, Baptista AJ, Rodrigues JD (2016) Reduced scale models based on similitude theory: A review up to 2015. *Eng Struct* 119:81–94
- Cremer L, Heckl M, Petersson BAT (2005) *Structural vibrations and sound radiation at audio frequencies*, 3rd edn. Springer, New York
- D'Alessandro V, Petrone G, De Rosa S, Franco F (2014) Modelling of aluminium foam sandwich panels. *Smart Struct Syst* 13(4):615–636
- De Rosa S, Franco F, Li X, Polito T (2012) A similitude for structural acoustic enclosures. *Mech Syst Signal Process* 30:330–342
- De Rosa S, Franco F, Mace BR (2005) The asymptotic scaled modal analysis for the response of a 2-plate assembly. *Volterra (PI), Italy*, pp 19–22. XVIII AIDAA National Congress
- De Rosa S, Franco F, Meruane V (2015) Similitudes for structural response of flexural plates. *Proc Instit MEchanical Eng Part C J MEchanical Eng Sci* 230(3):174–188
- Ewins DJ (2000) *Modal testing: Theory, practice and application*, 2nd edn. Wiley, Eastbourne (UK)
- Franco F, Robin O, Ciappi E, De Rosa S, Berry A, Petrone G (2019) Similitude laws for the structural response of flat plates under a turbulent boundary layer excitation. *Mech Syst Signal Process* 129:590–613
- Goodier JN, Thomson WT (1944) Applicability of similarity principles to structural models. Technical Report NACA Technical Report CR-4068, National Advisory Committee for Aeronautics Washington (DC) USA
- Jia Y, Yang Z, Liu E, Fan Y, Yang X (2020) Prediction of random dynamic loads using second-order blind source identification algorithm. *Proc IMechE Part C J Mechan Eng Sci* 234(9):1720–1732
- Jones EMC, Quintana EC, Reu PL, Wagner JL (2019) X-ray stereo digital image correlation. *Exp Tech* 44(2):159–174
- Kasivitanuay J, Singhatanadgid P (2005) Application of an energy theorem to derive a scaling law for structural behaviors. *Thammasat. Int. J. Sc Tech.* 10(4):33–40
- Kline SJ (1965) *Similitude and approximation theory*. McGraw-Hill, New York
- Li BJ, Wang QB, Duan DP (2019) Displacement measurement errors in digital image correlation due to displacement mapping function. *Exp Tech* 43(4):445–456

26. Luo Z, Wang Y, Zhu Y, Zhao X, Wang D (2015) The similitude design method of thin-walled annular plates and determination of structural size intervals. *Proc Instit Mechan Eng Part C J Mechan Eng Sci* 230(13):2158–2168
27. McNeill SI, Zimmerman DC (2008) A framework for blind modal identification using joint approximate diagonalization. *Mech Syst Signal Process* 22:1526–1548
28. Petrone G, D'Alessandro V, Franco F, De Rosa S (2014) Numerical and experimental investigations on the acoustic power radiated by aluminium foam sandwich panels. *Compos Struct* 118:170–177
29. Powell CA, Stephens DG (1966) Vibrational characteristics of sandwich panels in a reduced-pressure environment. Technical Report NASA TN D-3549, National Aeronautics and Space Administration, Langley Research Center, Langley Station, Hampton (VA) USA
30. Rezaeepazhand J, Simites GJ, Starnes JH Jr (1996) Design of scaled down models for predicting shell vibration response. *J Sound Vib* 195(2):301–311
31. Sarrafi A, Mao Z, Niezrecki C, Poozesh P (2018) Vibration-based damage detection in wind turbine blades using phase-based motion estimation and motion magnification. *J Sound Vib* 421:300–318
32. Siebert T, Becker T, Splitthof K, Neumann I, Krupka R (2007) Error estimations in digital image correlation technique. *Appl Mechan Mater* 7–8:265–270
33. Siebert T, Becker T, Splitthof K, Neumann I, Krupka R (2007) High-speed digital image correlation: Error estimations and applications. *Opt Eng* 46(5):051004–1–051004–7
34. Simites GJ, Rezaeepazhand J (1993) Structural similitude for laminated structures. *Compos Eng* 3(7–8):751–765
35. Simites GJ, Starnes JH Jr, Rezaeepazhand J (2000) Structural similitude and scaling laws for plates and shells: A review. pp 1–11, Atlanta (GA), USA, 3–6 April. 41st AIAA/ASME/ASCE/AHS/ASC Structures, Structural Dynamics, and Materials Conference and Exhibit
36. Torkamani S, Jafari AA, Navazi HM, Bagheri M (2009) Structural similitude in free vibration of orthogonally stiffened cylindrical shells. *Thin-Walled Struct* 47:1316–1330
37. Vinson JR (1999) The behavior of sandwich structures of isotropic and composite materials. Taylor and Francis Technomic Publishing Co, Lancaster
38. Zhihui Z, Sihui L, Qianshuo F, Yuanchang C, Fan W, Lizhong J (2020) A hybrid dic-efg method for strain field characterization and stress intensity factor evaluation of a fatigue crack. *Measurement* 154
39. Zhu Y, Luo Z, Zhao X, Wang D (2017) Similitude design for the vibration problems of plates and shells: A review. *Front Mech Eng* 12(2):253–264

Publisher's Note Springer Nature remains neutral with regard to jurisdictional claims in published maps and institutional affiliations.

